Transformation mechanisms of iopamidol by iron/sulfite systems: Involvement of multiple reactive species and efficiency in real water

Yuan Gao, Wenxia Fan, Zhong Zhang, Yang Zhou, Zhu Zeng, Kai Yan, Jun Ma, Khalil Hanna

Transformation mechanisms of iopamidol by iron/sulfite systems: involvement of multiple reactive species and efficiency in real water

Yuan Gao[a,c], Wenxia Fan[b], Zhong Zhang[b,c], Yang Zhou[b,c*],Zhu Zeng[b], Kai Yan[a], Jun Ma[d], Khalil Hanna[e*]

[a] School of Civil and Transportation Engineering, Guangdong University of Technology, Guangzhou 510006, Guangdong, China

[b]Key Laboratory for City Cluster Environmental Safety and Green Development of the Ministry of Education, School of Ecology, Environment and Resources, Guangdong University of Technology, Guangzhou, 510006, China

[c] Southern Marine Science and Engineering Guangdong Laboratory (Guangzhou), Guangzhou, 511458, China

[d] State Key Laboratory of Urban Water Resource and Environment, School of Environment, Harbin Institute of Technology, Harbin 150090, China

[e] Univ Rennes, Ecole Nationale Supérieure de Chimie de Rennes, UMR CNRS 6226, 11 Allée de Beaulieu, F-35708 Rennes Cedex 7, France.

*Corresponding Author: Yang Zhou and Khalil Hanna

Abstract

Although the ability of iron/sulfite system for decontamination purposes has been investigated, the complex reactive species generated and the underlying transformation mechanisms remain elusive. Here, we have comprehensively examined the transformation of iopamidol (IPM), a representative of iodinated X-ray contrast media, by iron catalyzed sulfite oxidation process under different water chemistry conditions. Multiple reactive intermediates including Fe(IV), $SO_4^{\bullet-}$, and $SO_5^{\bullet-}$ were identified by conducting a series of experiments. Eight transformation products were detected by mass spectrometry analysis, and correlation with the nature of involved reactive species has been made. Further, the transformation pathway including amide hydrolysis, deiodination, amino and hydroxyl groups oxidation was proposed. Interestingly, these transformation products could be removed through adsorption to iron precipitates formed via pH adjustment. Combining Fourier transform infrared spectroscopy and X-ray photoelectron spectroscopy, we revealed an effective way to reduce the amount of transformation products in the treated solutions. Since the iron/sulfite process appears to be less sensitive to natural organic matter, it exhibited very good efficiency for IPM removal in real water samples, even with a high organic carbon loading. These findings may have strong implications in the development of novel oxidation process based on the sulfite/iron systems for wastewater treatment.

Keywords

Iodinated X-ray contrast media; sulfur radicals; Fe(IV); organic carbon

1. Introduction

Iodinated X-ray contrast media (ICM), used for medical imaging of internal organs, blood vessels and soft tissues, are the most widely administered intravascular pharmaceuticals with the worldwide consumption of 3.5×10^6 kg per year (Duirk et al., 2011). This class of pharmaceuticals are specifically designed to be metabolically stable and almost completely excreted from the body via urine or faeces (Pérez et al., 2006). Due to their high solubility and poor biodegradability, conventional wastewater treatments are not effective in abating ICM, resulting in their occurrence in surface water and even drinking water ranging from ng L^{-1} to μg L^{-1} (Kormos et al., 2011; Putschew et al., 2000; Ternes and Hirsch, 2000; Xu et al., 2017). Iopamidol (IPM), a representative of ICM, is the most frequently detected at concentration level up to μg L^{-1}. Because of their high environmental concentrations and potential to leak through wastewater treatment plants and even reach drinking water, ICM has become chemicals of emerging concern to the public. Although ICM is believed not to be harmful, any subtle effects of mixtures, their metabolites, or other micropollutants are currently unknown and may pose ecological or human health issues (Ens et al., 2014). Considering their low biodegradability, ICM may also accumulate in the environment. Also, ICM might serve as the iodine source promoting the formation of iodinated by-products (Duirk et al., 2011; Pantelaki and Voutsa, 2018). For this reason, removal of ICM in water has been the subject of numerous studies (Cao et al., 2021; Chan et al., 2010; Jeong et al., 2010; Mao et al., 2020; Ternes et al., 2003; Tian et al., 2017; Wendel et al., 2014, Zhao et al., 2019).

Recently, ozone, chlorine, and chlorine dioxide were used as selective oxidant to remove ICM, which showed very limited efficiency with the maximum rate constant up the order of 10 $M^{-1}s^{-1}$ (Ternes et al., 2003; Tian et al., 2017; Wendel et al., 2014). However, hydroxyl (•OH) and sulfate radicals ($SO_4^{\bullet-}$) generated from UV/H_2O_2, O_3/H_2O_2 or O_3/PMS systems were found to be able to transform ICM compounds with the reaction rate constant of ~$10^9 M^{-1}s^{-1}$ (Chan et al., 2010; Jeong et al., 2010; Mao et al., 2020). As compared to •OH, $SO_4^{\bullet-}$ has been reported to be less influenced by natural organic matter in real water matrix (Gara et al., 2008; Lutze et al., 2015). Thus, sulfate radical based oxidation technologies could be considered as promising for ICM removal in wastewater.

Transition metal catalyzed sulfite is one of the possibilities for $SO_4^{\bullet-}$ generation through chain propagation reactions (Brandt et al., 1994; Yermakov and Purmal, 2003). As compared to persulfates (peroxydisulfate and peroxymonosulfate), commonly employed as $SO_4^{\bullet-}$ precursor, sulfite takes the advantage of lower toxicity and competitive price. For instance, the LD_{50} (oral, rat) of sulfite is 3560 mg/kg, three times higher than that of peroxydisulfate (802 mg/kg) (Zhou et al., 2018a). Among various transition metals, iron is the most widely used one for environmental application because of its cost effectiveness and environmentally friendly nature. This iron-catalyzed sulfite oxidation process in the atmospheric liquid phase has been extensively investigated due to its implication on the generation of acid rain (Brandt and van Eldik, 1995). Recently, the iron/sulfite system has been investigated for water contaminants removal (e.g., dyes, aniline, and carbamazepine) (Chen et al., 2012; Dong et al., 2020;

Yu et al., 2016; Yuan et al., 2019). In these studies, multiple reactive intermediates including $SO_4^{\bullet-}$, •OH and peroxornonosulfate radical ($SO_5^{\bullet-}$) were proposed to be the candidates of potential oxidant. For instance, Chen et al. (2012) reported that the efficient decolorization of orange II in the Fe(II)/sulfite system was mainly attributed to the contribution of $SO_4^{\bullet-}$, while •OH and $SO_5^{\bullet-}$ contribution were considered as minor. Other reports showed that the combination of Fe(II) or Fe(III) and sulfite could generated $SO_5^{\bullet-}$, $SO_4^{\bullet-}$ or •OH, and then effectively remove organic contaminants (Dong et al., 2020; Yuan et al., 2019). Although the good ability of the iron/sulfite system for contamination removal has been investigated, the underlying mechanisms of generation of reactive species and target compound degradation remain elusive. In addition, very little is known about the application of this process for ICM transformation, and much less on the influence of key factors (*e.g.*, pH and water matrix) on the removal performance.

In this work, the performance and mechanism of the iron/sulfite system for the degradation of IPM were investigated for the first time. The primary objectives of the present work were to (i) assess the oxidation efficiency of the iron/sulfite system in IPM transformation; (ii) identify the reactive intermediates responsible for IPM degradation; (iii) elucidate the reaction mechanism based on the identified oxidation products; (iv) evaluate the influence of pH adjustment of the resulting solutions and water matrix on the performance of the iron/sulfite system.

2. Experimental Section

2.1. Materials

All chemicals were of analytical purity or higher and used without further purification unless otherwise stated. IPM (98%) was obtained from Macklin Biochemical Co., Ltd. Sodium sulfite (Na_2SO_3; AR, ≥97.0%) and ethanol (AR, ≥ 95.0%) were purchased from Chemical Reagent Co. Ltd. Iron nitrate nonahydrate ($Fe(NO_3)_3 \cdot 9H_2O$, AR), ferrous sulfate heptahydrate ($FeSO_4 \cdot 7H_2O$; AR, ≥ 99.0%), and tert-butyl alcohol (TBA >99.5%) were purchased from Aladdin Biochemical Co., Ltd. Peroxymonosulfate (PMS, available as Oxone), methyl phenyl sulfoxide (PMSO, ≥ 97%) and methyl phenyl sulfone ($PMSO_2$; GC, ≥ 98%), humic acid (HA) and acetic acid for HPLC were obtained from Sigma-Aldrich. Methanol and acetonitrile of chromatographic grad were obtained from Merck KGaA. All solutions were prepared using deionized (DI) water (18.2 MΩ·cm) from a Millipore purification system. The stock solutions of HA were purified by repeated pH adjustment, filtration, and precipitation. Stock solutions of sulfite and ferrous sulfate were freshly prepared before experiments. Real water samples were taken from the filtered water of secondary effluent of Lijiao Wastewater Treatment Plant (located in Haizhu district of Guangzhou in China; Dissolved organic carbon (DOC) of 5.6 mg L^{-1}, UV_{254} absorbance of 0.075 cm^{-1}, Cl^- of 1.8 mM and pH of 7.3) and central lake in Guangzhou (GPS coordinate of 23°03'07.3"N/113°23'21.8"E; DOC of 12.6 mg L^{-1}, UV_{254} absorbance of 0.083 cm^{-1}, Cl^- of 1.6 mM and pH of 6.8). After filtering through glass fiber membranes, these water samples were stored at 4 °C.

2.2. Experimental procedure

Batch experiments were conducted in open beakers with 100 mL capacity under magnetic stirring. To initiate the reactions, predetermined amounts of iron ion (50 μM) and sulfite (300 μM) were simultaneously added into stirring solutions containing IPM and/or constituents (e.g., Cl^- and humic acid) of interest at desirable concentrations. At specific time intervals, reaction solution was sampled and quenched by excess methanol for the following measurement of IPM or the analysis of transformation products. Experiments in real waters were conducted following the similar procedure as that in synthetic solutions except that a relatively low concentration of IPM (500 nM) was used to simulate environmental levels.

Unless otherwise stated, the experiments in this study were conducted at controlled temperature (25 ± 1 °C) in ambient atmosphere. The solution pH was adjusted with $HClO_4$ and NaOH. To ensure reproducibility, the experiments were conducted in triplicates with results presented as the average data and the relative standard deviations were also presented.

2.3. Analytical Methods

IPM was quantified by using a Waters Alliance e2695 HPLC. The separation was achieved by a Waters XBridge C18 column (4.6×250 mm, 5μm particle size) and the mobile phase consisted of 0.1% acetic acid and methanol with a ratio of 90:10 (v/v) at a flow rate of 0.5 mL/min. The wavelength for IPM was set at 242 nm. PMSO and $PMSO_2$ were analyzed by HPLC/UV at 230 and 215 nm, with the eluent of 0.1% acetic acid and acetonitrile at a flow rate of 1 mL/min. A Sciex QTrap 5500 MS with an ESI source was used for products identification and quantification. The MS instrumental

parameters were provided in Text S1. Electron paramagnetic resonance (EPR) analysis using DMPO as a spin-trapping agent was performed on a Bruker A200 spectrometer, and the detailed parameters were shown in Text S2. Fourier transform infrared spectroscopy (FTIR) analysis was conducted on a Shimadzu IRTracer-100 and the samples was prepared by vacuum filtration via 0.45 μm filters. X-ray photoelectron spectrometer (XPS) was conducted on a Thermo Fisher Escalab 250Xi and the samples was prepared by vacuum filtration via 0.45 μm filters followed by vacuum drying. The DOC content of HA stock solution was determined using Shimadzu TOC-L. Solution pH was measured with Leici PHS–3C pH-meter (Shanghai INESA Scientific Instrument Co.Ltd). Dissolved oxygen was detected using Hach HQ40d Portable Meters. Absorbance was measured by Hach DR6000 Spectrophotometer.

3. Results and Discussion

3.1 Degradation of IPM by iron/sulfite

Figure 1 comparatively showed the degradation of IPM in the Fe/sulfite as well as Fe(II)/persulfates (PDS or PMS). The combination of Fe(III) (50 μM) and sulfite (300 μM) led to an efficient abatement of IPM (5 μM) at pH_{ini} 4, where ~85% removal of IPM was achieved. Interestingly, Fe(II)/sulfite exhibited a similar reactivity toward IPM removal. Comparatively, Fe(II)/PMS and Fe(II)/PDS systems only achieved ~40% removal under the same conditions. Similar findings were obtained in the case of diatrizoate, a relatively refractory ICM. The removal percentage of diatrizoate in the iron/sulfite system (~50%) was at least more than twice that in the Fe(II)/PMS and Fe(II)/PDS systems (<25%) (**Fig. 1**). These findings indicated the higher oxidation

efficiency of iron/sulfite system in ICM abatement as compared to commonly used iron-based Fenton-like AOPs.

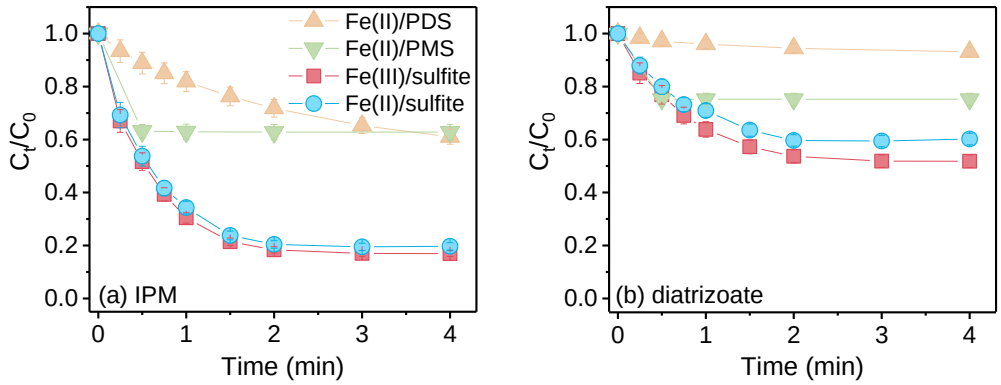

Fig. 1 Degradation of IPM (a) or diatrizoate (b) in the iron/sulfite and iron/persulfates systems. Experimental conditions: [IPM] = 5 μM, [Fe(II)] = [Fe(III)] = 50 μM, [sulfite] = [persulfates] (i.e., [PDS] or [PMS]) = 300 μM, and pH_{ini} = 4.

Further, the effect of pH_{ini} on the performance of Fe(III)/sulfite system was examined. It was found that efficiency of Fe(III)/sulfite system increased first as pH_{ini} increased from 3 to 4, and then decreased when pH_{ini} further increased and became negligible at higher pH values (7 and 9) (Fig. S1a). The pH variation was also measured and the solution pH at the end of reaction (pH_{final}) was shown in Figure S1b. To evaluate the reaction kinetics at different pH_{ini}, the initial reaction rates k_{ini} over the first reaction time (within 1 min) was determined. The k_{ini} value first increased from 0.80 to 1.23 min^{-1} as pH_{ini} increased from 3 to 4, and then decreased to 0.08 min^{-1} as pH further increased to pH_{ini} 9. This could be probably due to the combined effect of pH on the distribution of sulfite species and iron speciation in solution (Guo et al., 2013). Acidic pH may facilitate the formation of sulfur dioxide, thus decreasing the effective concentration of HSO_3^-. At higher pH, iron precipitation takes place, thereby decreasing the dissolved iron concentration available for sulfite activation.

3.2 Identification of reactive radical species

Preliminary experiments showed that negligible degradation of IPM was observed in the case of Fe(III) or sulfite alone (Fig. S2). Therefore, Fe(III)-induced activation of sulfite is likely to occur for the generation of reactive species. A radical mechanism has been well reported for the complex reaction of Fe(III) catalyzed sulfite auto-oxidation (eqs. 1-12) (Brandt et al., 1994). The fast formation of Fe(III)-sulfito complex ($K_{Fe(III)\text{-}sulfito} = 600$) and its subsequent decomposition to Fe(II) and $SO_3^{\bullet-}$ is considered as the core of the reactions (eqs. 1-2), which participate to the generation of $SO_3^{\bullet-}$ as the initiation step of catalytic sulfite oxidation. In the present work, the degradation of IPM was completely inhibited with the addition of EDTA and pyrophosphate, stronger chelators for iron (e.g., $K_{Fe(III)\text{-}EDTA} = 10^{24.23}$) (Fig. S3). Then, the generated $SO_3^{\bullet-}$ may combine quickly with oxygen (O_2) leading to the formation of $SO_5^{\bullet-}$ (eq. 3). This reactive species may oxidize either sulfite or Fe(II) resulting in the production of sulfur-containing intermediates including $SO_4^{\bullet-}$, $SO_3^{\bullet-}$ and HSO_5^- (peroxymonosulfate ion) (eqs. 4-6). These intermediates could further induce several redox processes such as oxidizing sulfite or Fe(II) (eqs. 7-12). This was consistent with the evolution of sulfite (continuous degradation) and Fe(II) (initial increase concentration and then decrease) observed during the reaction in the present study (Fig. S4). In addition, •OH might be generated from the reaction of $SO_4^{\bullet-}$ and H_2O (Neta et al., 1988).

$$Fe^{3+} + HSO_3^- \overset{K=600}{\longleftrightarrow} FeSO_3^+ + H^+ \quad (1)$$

$$FeSO_3^+ \rightarrow Fe^{2+} + SO_3^{\bullet-} \quad (2)$$

$$SO_3^{\bullet-} + O_2 \rightarrow SO_5^{\bullet-} \quad (3)$$

$$SO_5^{\bullet-} + HSO_3^- \rightarrow SO_4^{\bullet-} + SO_4^{2-} + H^+ \quad (4)$$

$$SO_5^{\bullet-} + HSO_3^- \rightarrow SO_3^{\bullet-} + HSO_5^- \quad (5)$$

$$SO_5^{\bullet-} + Fe^{2+} \rightarrow Fe^{3+} + HSO_5^- \quad (6)$$

$$HSO_5^- + HSO_3^- \rightarrow SO_3^{\bullet-} + SO_4^{\bullet-} + H_2O \quad (7)$$

$$HSO_5^- + HSO_3^- \rightarrow +2SO_4^{2-} + 2H_2O \quad (8)$$

$$HSO_5^- + Fe^{2+} \rightarrow Fe^{3+} + SO_4^{\bullet-} + OH^- \quad (9)$$

$$SO_4^{\bullet-} + HSO_3^- \rightarrow SO_3^{\bullet-} + SO_4^{2-} + H^+ \quad (10)$$

$$SO_4^{\bullet-} + Fe^{2+} \rightarrow Fe^{3+} + SO_4^{2-} \quad (11)$$

$$SO_4^{\bullet-} + H_2O \rightarrow \bullet OH + SO_4^{2-} + H^+ \quad (12)$$

In the case of Fe(II), a rapid formation of $FeSO_3^+$ is possible (eqs. 13-14) (Chen et al., 2012; Guo et al., 2013), which would in turn follow the same reaction chain (eqs. 2-12). Therefore, the same reactive species should be involved in Fe(II)/sulfite and Fe(III)/sulfite systems, thereby explaining their similar performance in IPM degradation as observed in Figure 1a.

$$Fe^{2+} + HSO_3^- \leftrightarrow FeHSO_3 \quad (13)$$

$$4FeHSO_3 + O_2 \rightarrow 4FeSO_3^+ + 2H_2O \quad (14)$$

3.2.1 Role of $SO_4^{\bullet-}$ and •OH in IPM degradation

According to eqs. 1-12, $SO_4^{\bullet-}$ and •OH were usually considered as the primary reactive species responsible for contaminant degradation in the iron ions/sulfite system (Chen et al., 2012; Dong et al., 2020). To gain further insights into the role of $SO_4^{\bullet-}$ and •OH in IPM degradation, alcohol scavenging experiments were conducted. The inhibitory effects of ethanol and TBA (commonly used scavengers) could be used as a mean to

verify the contribution of $SO_4^{\bullet-}$ and •OH. Ethanol could react quickly with both $SO_4^{\bullet-}$ and •OH with the rate constants of 1.6-7.7 × 10^8 $M^{-1}s^{-1}$ and 1.2-2.8 × 10^9 $M^{-1}s^{-1}$ (Buxton et al., 1988; Neta et al., 1988). TBA could effectively scavenge •OH with the rate 3.8-7.6 × 10^8 $M^{-1}s^{-1}$, which was about 3 orders of magnitude higher than the rate constant for the reaction of TBA and $SO_4^{\bullet-}$ (4.0-9.1 × 10^5 $M^{-1}s^{-1}$) (Buxton et al., 1988; Neta et al., 1988). The rate constants for the reaction of IPM with •OH and $SO_4^{\bullet-}$ are 3.4 × 10^9 $M^{-1}s^{-1}$ and 1.6 × 10^9 $M^{-1}s^{-1}$ as reported in literature (Jeong et al., 2010; Mao et al., 2020). Theoretically, the addition of 5 mM TBA or 50 mM ethanol could almost completely suppress the degradation of IPM (5 μM) by •OH or $SO_4^{\bullet-}$ ($k_{OH^{\bullet}\text{-TBA}}[TBA] > 100k_{OH^{\bullet}\text{-IPM}}[IPM]$, $k_{SO_4^{\bullet-}\text{-ethanol}}[ethanol] > 100k_{SO_4^{\bullet-}\text{-IPM}}[IPM]$; details in Text S3). As shown in **Figure 2a**, 5 mM TBA slightly affected the degradation of IPM, excluding the involvement of •OH. This might be due to the slow formation rate of $SO_4^{\bullet-}$ from the reaction of •OH with water (<6 M^{-1} s^{-1}, eq. 12). This finding was also confirmed by the EPR analysis where characteristic spectrum of the hydroxyl radical was not observed in the Fe(III)/sulfite system (**Fig. 2b**). Comparatively, ethanol considerably suppressed the degradation of IPM, suggesting the possible involvement of $SO_4^{\bullet-}$. Although the signal of DMPO/$SO_4^{\bullet-}$ was not observed, the characteristic spectrum of EPR analysis for the DMPO/$SO_3^{\bullet-}$ adduct (α^N = 14.7 G, α^H = 15.9 G) was detected (**Fig. 2b)** (Mottley and Mason, 1988). The absence of DMPO/$SO_4^{\bullet-}$ signal might be due to the high concentration of DMPO, which could completely trap $SO_3^{\bullet-}$ and thus inhibited $SO_4^{\bullet-}$ generation (eqs 3-9) (Yuan et al., 2016). Interestingly, ~15% IPM removal was still achieved in the presence of 50 mM ethanol, suggesting that other reactive species could

be involved in the Fe(III)/sulfite system.

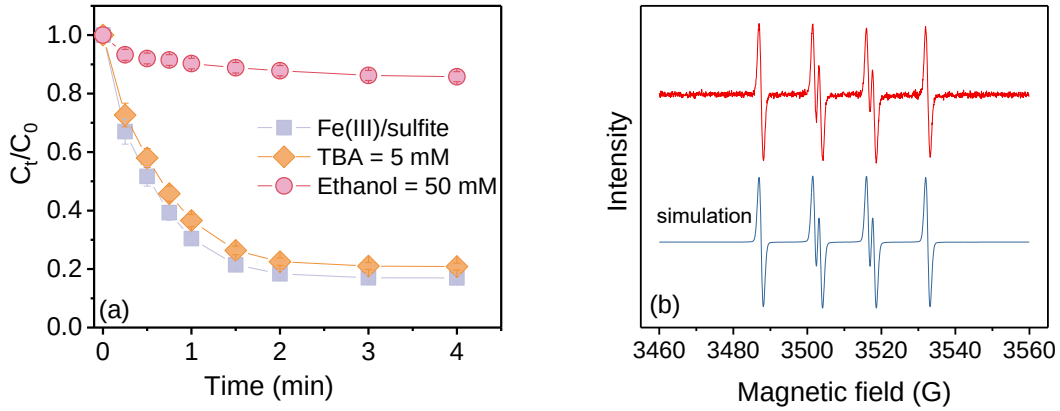

Fig. 2 Effect of alcohol scavengers on IPM degradation in the Fe(III)/sulfite system as well as the EPR spectra obtained from the Fe(III)/sulfite/DMPO system (red line) and the simulation of DMPO-$SO_3^{\bullet-}$ adduct (blue line). Experimental conditions: [IPM] = 5 μM, [Fe(III)] = 50 μM, [sulfite] = 300 μM, pH_{ini} = 4, and [TBA] = 5 mM, [ethanol] = 50 mM for (a),or [DMPO] = 10 mM for (b).

3.2.2 Role of Fe(IV) in IPM degradation

In previous studies, the reaction of HSO_5^- (*i.e.*, monoanion form of PMS) and Fe(II) depicted as eq. 9 was usually considered as the main source for $SO_4^{\bullet-}$ in the Fe(III)/sulfite system (Chen et al., 2012; Dong et al., 2020). However, Fe(IV) has been reported to be the primary oxidant in the Fe(II)/PMS, generated from Fe(II) and HSO_5^-, in a recent work (Wang et al. 2018) (eq. 15). This Fe(IV) generation has been proposed based on conversion reaction of methyl phenyl sulfoxide (PMSO) to methyl phenyl sulfone ($PMSO_2$) via oxygen electron transfer. Comparatively, $PMSO_2$ was not generated in the case of free radicals (Wang et al. 2018).

$$HSO_5^- + Fe(II) \rightarrow Fe(IV) + SO_4^{2-} \quad (15)$$

Thus, it is quite plausible that Fe(IV) was involved in the Fe(III)/sulfite system generated from eq. 15. In order to verify this possibility, the degradation of methyl phenyl sulfoxide (PMSO) in the Fe(III)/sulfite system was examined. As expected, the

formation of methyl phenyl sulfone ($PMSO_2$) (1.1 μM) was observed from the transformation of 2.8 μM PMSO, suggesting the involvement of other reactive intermediates (possibly Fe(IV)) in the Fe(III)/sulfite system.

Fe(IV) is known to serve as an oxidant with considerable selectivity. For instance, the rate constants for the reaction of Fe(IV) with phenol and dimethyl sulfoxide (DMSO) were reported to be k_{phenol} = 4 × 10^3 $M^{-1}s^{-1}$ and k_{DMSO} = 1.26 × 10^5 M^{-1} s^{-1}, respectively (Jacobsen et al., 1998; Mártire et al., 2002). To evaluate the oxidizing ability of Fe(IV) toward IPM, the degradation of IPM in the Fe(II)/PMS and Fe(II)/HOCl systems was examined, wherein Fe(IV) has been reported to be the primary oxidant (Fig.3 and Fig. S5). Significant IPM degradation was observed suggesting that Fe(IV) could contribute to IPM removal in the Fe(III)/sulfite system.

Interestingly, 50 mM ethanol was found to completely inhibit the degradation of IPM in the Fe(II)/PMS system (**Fig. 3**), underscoring the role of ethanol as an effective scavenger for Fe(IV). This was also consistent with previous work on the inhibitory effect of ethanol on the Fe(II)/ozone and Fe(II)/HOCl systems, where Fe(IV) served as the main reactive intermediates (Liang et al., 2020; Pestovsky and Bakac, 2004). However, partial inhibition was observed in the Fe(III)/sulfite system upon addition of 50 mM ethanol (**Fig. 2a**), suggesting that other reactive intermediates, in addition to $SO_4^{\bullet-}$ and Fe(IV), may exist in the Fe(III)/sulfite system.

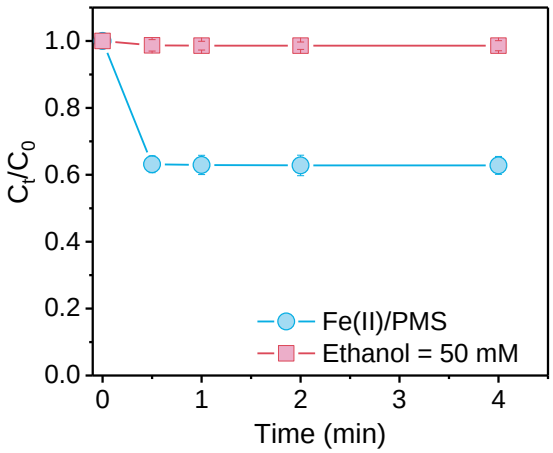

Fig. 3 Effect of alcohol scavengers on IPM degradation in the Fe(II)/PMS. Experimental conditions: [IPM] = 5 μM, [Fe(II)] = 50 μM, [PMS] = 300 μM, pH_{ini} = 4, and [ethanol] = 50 mM.

3.2.2 Role of HSO_5^-, $SO_3^{\bullet-}$ and $SO_5^{\bullet-}$ in IPM degradation

Recently, HSO_5^- (*i.e.*, monoanion form of PMS) was found to be a mild oxidant towards organic compounds such as estrogens and antibiotics with the rate constants ranging from 0.5-30 $M^{-1}s^{-1}$ (Zhou et al., 2018b, 2018c). Here, the degradation of IPM by HSO_5^- was found negligible (**Fig. 4a**), ruling out the contribution of HSO_5^- to IPM degradation in the iron/sulfite system. $SO_3^{\bullet-}$ with a redox potential of $E(SO_3^{\bullet-}/HSO_3^-)$ = 0.84 V (vs. NHE) could act as a weak oxidant or a strong reductant (Neta and Huie, 1985a). Experiments were conducted in anaerobic condition to examine the reactivity of $SO_3^{\bullet-}$ toward IPM. Less than 10% of IPM was degraded in the absence of O_2, where $SO_3^{\bullet-}$ served as the predominant oxidant (**Fig. 4b**), underscoring the minor role of $SO_3^{\bullet-}$ in IPM degradation. However, it should be noted that $SO_3^{\bullet-}$ could quickly react with O_2 with the second-order rate constant up to 2.5×10^9 $M^{-1}s^{-1}$ as described in eq. 3 (Fronaeus et al., 1998). The evolution of dissolved O_2 during the reaction was also monitored (**Fig. 4c**). The initial decrease of O_2 further confirmed the participation of O_2 (eq. 3) in the

316 Fe(III)/sulfite oxidation process, while further increase of O_2 level might be due to the
317 redissolution of O_2 under open atmosphere. Given the fast reaction of $SO_3^{\bullet-}$ with O_2
318 and the relatively high concentration of dissolved O_2 (⩾155 μM under atmospheric
319 pressure), $SO_3^{\bullet-}$ would be quickly reacted with O_2 rather than with IPM.

320 $SO_5^{\bullet-}$, a relatively stronger oxidant, has been reported to react effectively with
321 several organics such as aromatic amines and hydroxyphenols (Huie and Neta, 1984;
322 Neta and Huie, 1985b). For instance, the rate constants for the reaction of Trolox with
323 $SO_5^{\bullet-}$ was reported to be 1.2×10^7 M^{-1} s^{-1}, more than 10 times the rate constant for the
324 $SO_3^{\bullet-}$ reaction (~10^6 M^{-1} s^{-1}). Therefore, $SO_5^{\bullet-}$ might also participate in IPM oxidation
325 in the Fe(III)/sulfite system. In contrast to $SO_4^{\bullet-}$ and Fe(IV), $SO_5^{\bullet-}$ is relatively inert
326 toward ethanol with a low rate constant, ~10^3 $M^{-1}s^{-1}$ (Neta et al., 1988). Thus, the IPM
327 degradation (~15%) observed in excess ethanol (**Fig. 2a**) could be resulted from the
328 contribution of $SO_5^{\bullet-}$. Diphenylamine (DPA) with a relatively higher rate constant with
329 $SO_5^{\bullet-}$ is usually used as scavenger to terminate the contribution of $SO_5^{\bullet-}$ (Neta and Huie,
330 1985b; Yuan et al., 2019). Here, the effect of DPA on IPM degradation in the
331 Fe(III)/sulfite system was examined. In contrast to the partial inhibitory effect of
332 ethanol, IPM was completely suppressed in the presence of 50 μM DPA (**Fig.4d**),
333 further suggesting the role of $SO_5^{\bullet-}$ in IPM degradation in the iron/sulfite system.

334 Taken together, these findings suggest that multiple reactive species including
335 Fe(IV), $SO_4^{\bullet-}$, and $SO_5^{\bullet-}$ could contribute to the IPM transformation in the iron/sulfite
336 system.

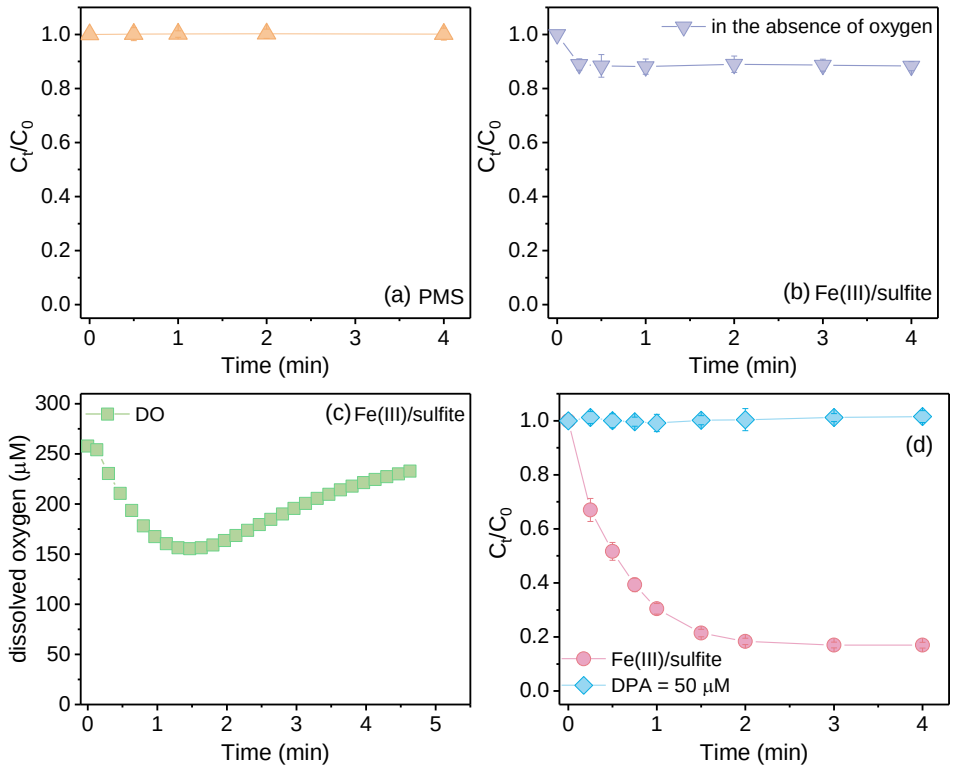

Fig. 4 Oxidation of IPM by PMS under open atmosphere (a), by Fe(III)/sulfite system in the absence of oxygen (b), evolution of oxygen during Fe(III)/sulfite system and effect of DPA on the degradation of IPM in the Fe(III)/sulfite system under a open atmosphere. Experimental conditions: [IPM] = 5 μM, [Fe(III)] = 50 μM, [sulfite] = 300 μM, pH_{ini} = 4, and [PMS] = 300 μM for (a), or [DPA] = 50 μM for (d).

3.4 Transformation mechanism

ESI−MS at precursor ion scan (PIS) mode was used to selectively detect polar halogenated compounds. Given three iodine atoms in IPM, this approach setting precursor ion at m/z 127 was used to detect the primary transformation products of IPM in the Fe(III)/sulfite system. **Figure 5** showed the HPLC/ESI-MS chromatogram of IPM after the treatment of Fe(III)/sulfite with eight new peaks corresponding to transformation products (TPs). These TPs were further identified based on their molecular mass and MS/MS fragmentations. For instance, TP 1 eluting at 7.21 min had the molecular ion of m/z 667, 110 Da loss as compared to IPM of m/z 777 (as

353 [$C_{17}H_{22}I_3N_3O_8$]) with the retention time of 8.22 min. This product was proposed to be
354 a hydroxylated product $C_{17}H_{23}I_2N_3O_9$, consistent with the nitrogen rule and its
355 fragments observed in the product ion scan spectra. The fragment ions of 72 (-CO-
356 CHOH-CH_2), 263 (-CO-CHOH-CH_2-, -CH-CH_2OH-CHOH-, -CO-NH-CH-CH_2OH-
357 CHOH-) indicated the intact acylamino side chain A and carboxamide side chains B.
358 TP 2 at the retention time of 11.73 min has the molecular ion of m/z 705. Two major
359 products m/z 587 (-117) and m/z 467 (-324) were observed in its product ion scan
360 spectra, corresponding to the successive loss of two side chain B (-CO-NH-CH-
361 CH_2OH-CHOH-). This finding indicated carboxamide side chains were intact in this
362 product and it might be generated from the cleavage of C-N bond in the amide moiety
363 of acylamino side chain A. Following similar procedure, other TPs were identified (Fig.
364 S6-S11) and their information including retention time, molecular mass, chemical
365 formula and proposed molecular structure were shown in **Table 1**.

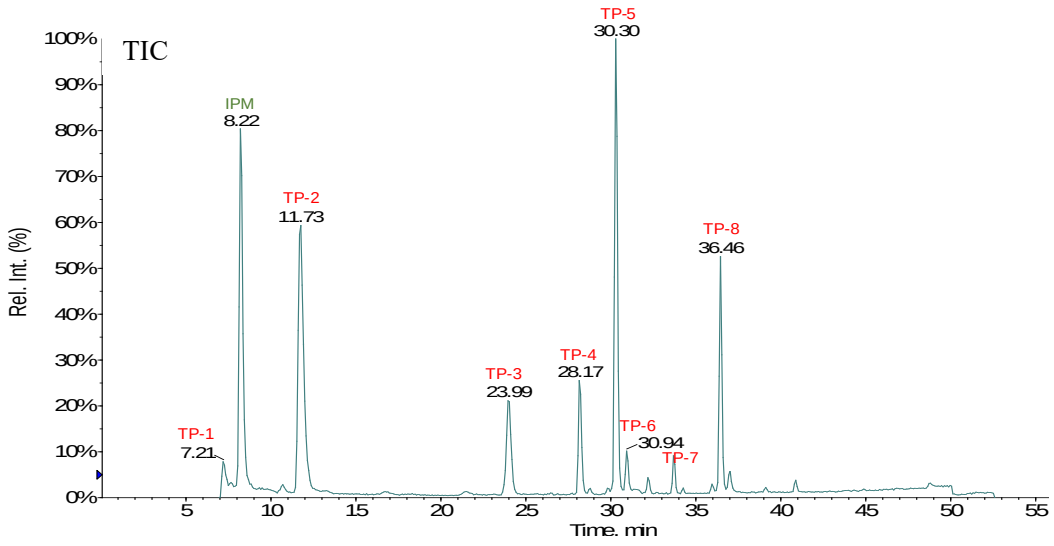

366

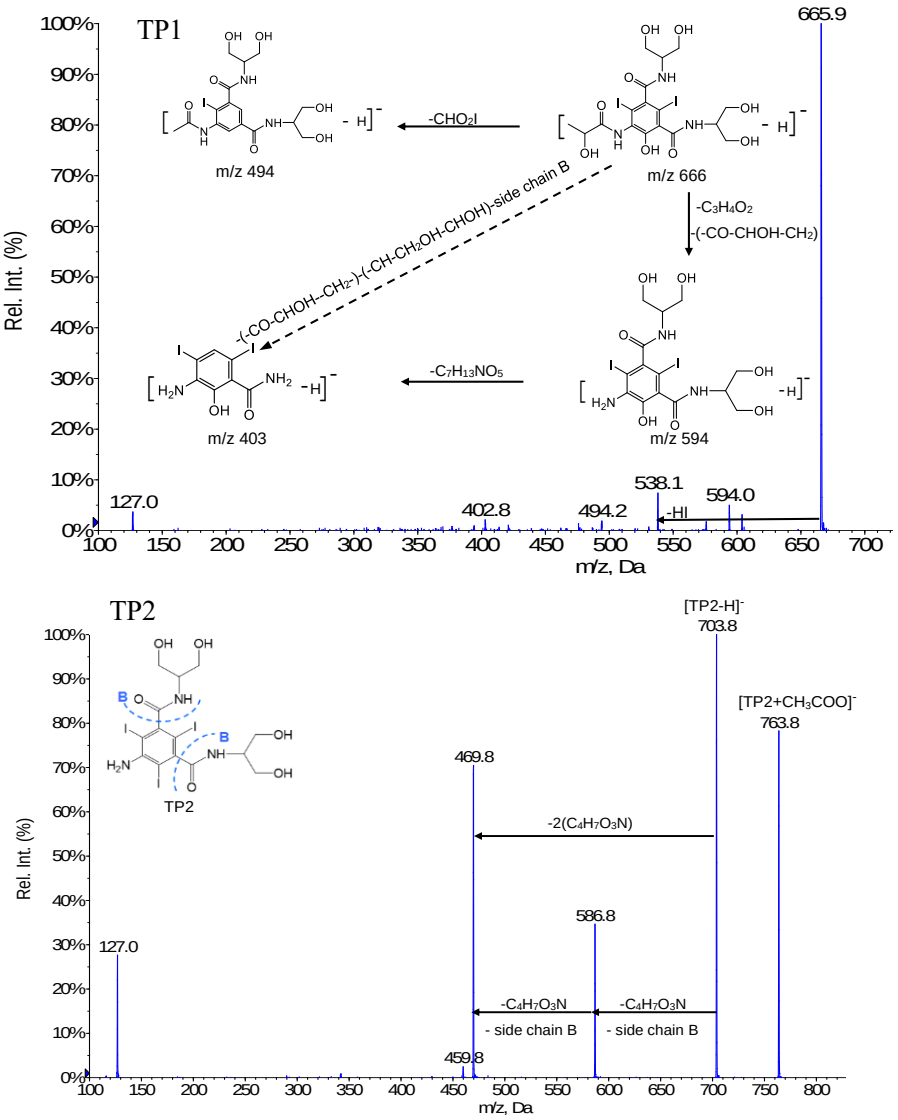

Fig.5 The HPLC/ESI-MS chromatograms of IPM after the treatment of Fe(III)/sulfite and fragmentation pattern of TP-1 and TP-2. Experimental condition: [IPM] = 5 μM, [Fe(III)] = 50 μM, [sulfite] = 300 μM, and pH_{ini} = 4

To further understand the transformation pathway, the transformation products of IPM by $SO_4^{\bullet-}$, $SO_5^{\bullet-}$, and Fe(IV) were comparatively detected. Figure S12 exhibited the HPLC/ESI-MS chromatograms of IPM after the treatment of Heat/PDS, which has been acknowledged as the common approach for $SO_4^{\bullet-}$ production (Johnson et al., 2008; Lee et al., 2020). The production of TP 2-6 was observed, indicating the oxidation role of $SO_4^{\bullet-}$. To explore the TPs of IPM by $SO_5^{\bullet-}$, experiments were conducted in the presence of 50 mM ethanol, where the contribution of $SO_4^{\bullet-}$ and Fe(IV) could be

terminated and $SO_5^{\bullet-}$ would act as the sole oxidant. TP 1-5 were generated indicated the $SO_5^{\bullet-}$ role in the formation of these products (Fig. S13). Further, the transformation products of IPM in the Fe(II)/PMS system were also detected to distinguish the products generated from Fe(IV) in the Fe(III)/sulfite system (Fig. S14). As expected, the generation of TP 7 and 8 other than TP 1-6 were observed in the case of Fe(IV), further indicating the participation of Fe(IV) in IPM degradation during Fe(III)/sulfite process. In addition, the difference in the production formation in the Heat/PDS system (acknowledged $SO_4^{\bullet-}$ system) and Fe(II)/PMS system again indicated the involvement of Fe(IV) in the Fe(II)/PMS system, supporting the formation of Fe(IV) from the reaction of Fe(II) and HSO_5^- (eq 15).

The time course profiles of products identified in the Fe(III)/sulfite were also monitored by HPLC/ESI MS at multiple reaction monitoring (MRM) mode. As could be seen in Figure S15, the formation of TP 1 (MW 667) and TP 3 (MW 731) was followed by their decay over time. The other products were gradually accumulated and reached plateau during the reaction time, which could be generated from the oxidation of TP 1 and TP 3 in the Fe(III)/sulfite system. Here, due to the lack of commercial standards, we cannot determine the absolute concentration of each TP, and only peak areas were used for data interpretation.

Based on these identified products, the transformation mechanism for IPM oxidation by the Fe(III)/sulfite system was tentatively proposed as shown in **Figure 6**. IPM would likely be oxidized by Fe(IV) or $SO_5^{\bullet-}$ leading to the formation of hydroxylated TP 1 (MW667), which was further transformed to TP 6 (MW 661) via

the cleavage of C-N bond in the amide moiety of acylamino side chain A. In parallel, IPM could be attacked by $SO_4^{\bullet-}$, $SO_5^{\bullet-}$ or Fe(IV) at the acylamino side chain and thus TP 2 (MW 705) could be generated from IPM by the cleavage of side chain A at the amide C-N bond. Subsequently, TP 5 (MW 735) is likely generated from TP 705 through amino groups oxidation to a nitro group, which further transforms to TP 7 (MW 719) via amide hydrolysis at amide C-N bond of side chains B. The oxidation of hydroxyl groups to carbonyl groups occurs in TP 5 and TP 7, leading to the formation of TP 3 (MW 731) and TP 4 (MW 659). Also, TP 2 (MW 705) may be transformed by Fe(IV) through hydroxyl groups oxidation into TP 8 (MW 689) with carboxylic group.

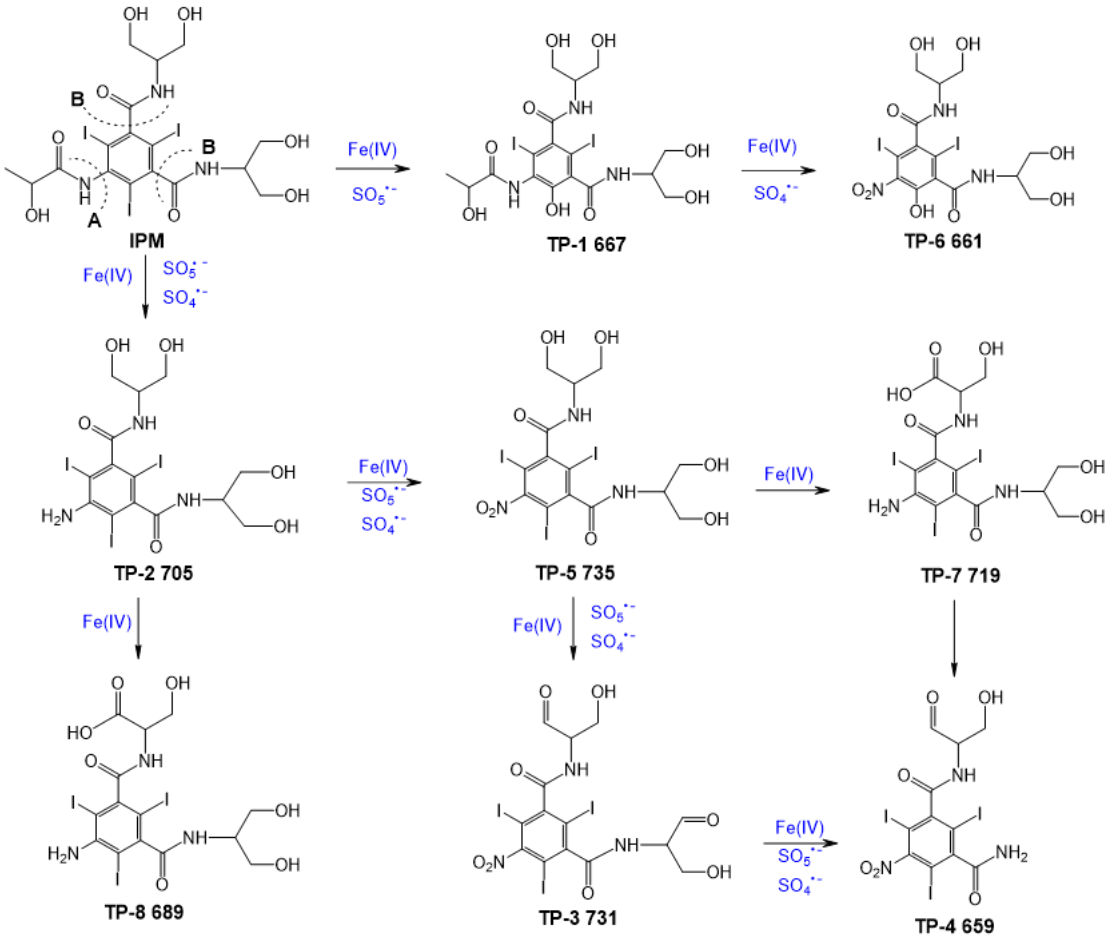

Fig. 6 Proposed pathway of IPM in the Fe(III)/sulfite process.

3.5 Removal of TPs from solutions via pH adjustment

Considering the hydrolysis of iron ion in neutral and alkaline conditions, the formation of iron precipitates through pH adjustment increasing up to neutral 7 and their removal capability towards transformation products were investigated. Interestingly, TP 3, TP 4, TP 7, TP 8 was not detected after pH adjustment to 7. The concentration of iodide before and after pH adjustment was also compared. An efficient iodide removal (~80%) was also observed, where the iodide in solutions decreased from 1.8 μM to 0.3 μM after pH adjustment (Fig.S16). These findings indicated that the transformation products of IPM as well as the iodide released from IPM during iron/sulfite process might be effectively removed through adsorption and/or coprecipitation with iron species. To further confirm this, FTIR and XPS were conducted to characterize the precipitates obtained in the Fe(III)/sulfite system after the pH adjustment. In the control group without IPM, the FTIR band recorded at 3400 and the peak at 1640 cm^{-1} were ascribed to the OH stretching vibration of water molecules (Fig. S17). The peak around 1300 cm^{-1} could be ascribed to the antisymmetric stretching of NO_3^- (resulting from the iron salt used, $Fe(NO_3)_3$). The peak near 800 cm^{-1} could be related to the OH bending modes in FeOOH (Amini et al., 2021). In the presence of IPM, the new peaks around 2900 cm^{-1} were ascribed to the alkane C-H. Also, the band around 1050 might be ascribed to C-OH stretching vibration or =CH (Saptari, 2003). The variation observed in the FTIR spectra with *vs* without IPM addition might be resulted from the alkane and alcohol functional groups or aromatic ring present in the transformation products. XPS analysis also indicated that Fe^{III}–precipitates were indeed generated in the Fe(III)/sulfite system via pH adjustment (Fig. S18). The peaks around 711 and 725 eV could be

attributed to Fe $2p_{3/2}$ and Fe $2p_{1/2}$ (Richardson and Johnston, 2007; Yang et al., 2021). No difference was observed in presence or absence of IPM, possible due to the low relative amount of organic products as compared to precipitates. Collectively, these results showed that adsorption of iodide-containing transformation products and iodide to iron precipitates could be considered as a way to reduce the to reduce the amount of transformation products in the treated solutions.

3.6 Effects of water matrix

Figure 7a showed the effect of water matrix including Cl^- and humic acid (surrogate of NOM) on the degradation of IPM in the Fe(III)/sulfite system. The presence of Cl^- suppressed the degradation of IPM to a certain extent. With the concentration of Cl^- increasing from 0 to 3 mg/L, the percentage of IPM degradation decreased from 85% to 50%. Comparatively, the effect of Cl^- on heat/PDS (for $SO_4^{\bullet-}$ generation) and Fe(II)/PMS systems was investigated. An inhibitory effect of Cl^- was observed in the scenario of heat/PDS (Fig. S19). In previous studies, it has been documented that Cl^- could act as a radical scavenger for $SO_4^{\bullet-}$ (eqs 16-17) with the formation of chlorine radicals ($Cl^{\bullet}$ and $Cl_2^{\bullet-}$) (Neta et al., 1988).

$$SO_4^{\bullet-}+Cl^- \rightarrow Cl^{\bullet}+SO_4^{2-} \quad (16)$$

$$Cl^{\bullet}+Cl^- \rightarrow Cl_2^{\bullet-}+SO_4^{2-} \quad (17)$$

The rate constant for the reaction of $Cl_2^{\bullet-}$ with IPM was estimated to be 2.5×10^6 $M^{-1}s^{-1}$, three orders of magnitude lower than that for the reaction of $SO_4^{\bullet-}$ with IPM (Zhao et al., 2019). The inhibitory effect of Cl^- on heat/PDS system further suggested the relatively lower reactively of chlorine radicals towards IPM as compared to $SO_4^{\bullet-}$. In

contrast, no difference in IPM degradation was observed in the Fe(II)/PMS system with or without Cl^- (Fig. S20). This distinct difference in the impact of Cl^- on Fe(II)/PMS vs heat/PDS system might be another indication for that Fe(IV) was the primary oxidant in the Fe(II)/PMS system, otherwise a inhibitory effect should be observed. In turn, this findings indicated that Cl^- has slight effect on Fe(IV) oxidation toward IPM. So, the inhibitory effect of Cl^- on the iron/sulfite system involving multiple reactive intermediates might be explained by that Cl^- captured $SO_4^{\bullet-}$ and chlorine radicals was less reactive toward IPM as compared to $SO_4^{\bullet-}$. Based on above findings, we could speculate that the effect of Cl^- on the iron/sulfite system was likely related to the reactivity of chlorine radicals towards contaminants.

As shown in **Figure 7b**, the degradation of IPM was slightly affected by humic acid (HA), where the percentage of IPM degradation stayed at ~80% when humic acid amount increased from 0.3 to 3 mg C/L. This finding indicated that the oxidation of IPM by reactive intermediates involved in the Fe(III)/sulfite system are slightly affected by HA.

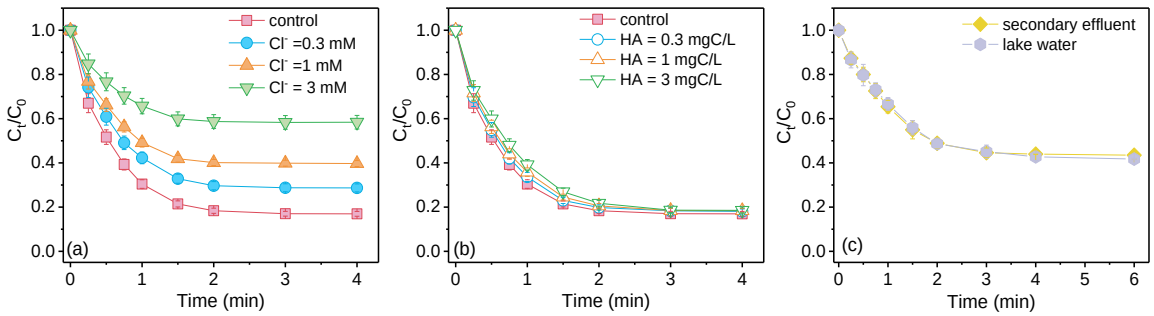

Fig. 7 Effect of chloride (a) and humic acid (b) on the degradation of IPM by the Fe(III)/sulfite system as well as the degradation of IPM in real water samples (c). Experimental condition: [Fe(III)] = 50 μM, [sulfite] = 300 μM, pH_{ini} = 4, [IPM] = 5 μM for (a) and (b), [IPM] = 500 nM for (c) to simulate environmental levels.

Further experiments were conducted to evaluate the performance of Fe(III)/sulfite system in two real water matrixes. As shown in **Figure 7c**, ~65% of IPM removal were achieved in both filtered secondary effluent and lake water samples. Since these water samples have similar chloride content but differ in organic carbon content (DOC 5.6 mg L^{-1}, Cl^- 1.8 mM for secondary effluent, whereas DOC 12.6 mg L^{-1}, Cl^- 1.6 mM for central lake), these results corroborate the above-mentioned findings, *i.e*. the efficiency of iron/sulfite system is less sensitive to natural organic matter, compared to chloride ions. Collectively, these results suggest that the Fe(III)/sulfite system is highly selective and effective for IPM removal, and could be applied in real waters containing high organic carbon content.

4. Conclusion

In this work, the performance of iron/sulfite system in IPM transformation as well as the mechanism were examined for the first time. Effective abatement of IPM was achieved by the iron/sulfite system, and the removal percentage was at least more than twice as compared to Fe(II)/PMS and Fe(II)/PDS systems. Multiple reactive species including Fe(IV), $SO_4^{\bullet-}$, and $SO_5^{\bullet-}$ contributed to the degradation of IPM in the iron/sulfite system. The transformation pathways including amide hydrolysis, deiodination, amino and hydroxyl groups oxidation were proposed for the degradation of IPM based on the identification of a total of eight transformation products. In addition, iron precipitates generated via pH adjustment could effectively remove transformation products as well as the iodide in the resulting solutions. In contrast to Cl^-, humic acid had a negligible impact on the IPM removal in the Fe(III)/sulfite system.

As a result, the iron/sulfite process exhibited a good efficiency for IPM removal in real water samples, even with a high organic carbon loading. Considering the low cost and good performance of the iron ions/sulfite system, this advanced oxidation process may be considered as a promising technology and an alternative for Fenton-like AOPs (Fe(II)/PMS and Fe(II)/PDS) in remediation of contaminated wastewater. In addition, this novel technology might be used as a possible pre-oxidation of IPM, in order to reduce the potential formation of iodinated by-products originated from ICM.

Acknowledgments

This study was financially supported by the National Natural Science Foundation of China (52000038 and 21906030), the Program for Guangdong Introducing Innovative and Entrepreneurial Teams (2019ZT08L213), the Guangdong Basic and Applied Basic Research Foundation (2019A1515110321 and 2019A1515011947), the Guangzhou Science and Technology Project (202002030093), the Open Project of State Key Laboratory of Urban Water Resource and Environment, Harbin Institute of Technology (No.HC202145), the Key Special Project for Introduced Talents Team of Southern Marine Science and Engineering Guangdong Laboratory (GML2019ZD0403). Thanks for the kind help of Dr. Tao Yang, Wei Song, Hang Bai and Zhengheng Yang regarding the XPS、EPR and FTIR analysis

Reference

Amini, M., Mousazade, Y., Zand, Z., Bagherzadeh, M., and Najafpour, M.M. (2021). Ultra-small and highly dispersive iron oxide hydroxide as an efficient catalyst for oxidation reactions: a Swiss-army-knife catalyst. Scientific Reports *11*, 6642.

Brandt, Christian., and van Eldik, Rudi. (1995). Transition Metal-Catalyzed Oxidation of Sulfur(IV) Oxides. Atmospheric-Relevant Processes and Mechanisms. Chem. Rev. *95*, 119–190.

Brandt, C., Fabian, I., and van Eldik, R. (1994). Kinetics and Mechanism of the Iron(III)-catalyzed Autoxidation of Sulfur(IV) Oxides in Aqueous Solution. Evidence for the Redox Cycling of Iron in the Presence of Oxygen and Modeling of the Overall Reaction Mechanism. Inorg. Chem. *33*, 687–701.

Buxton, G.V., Greenstock, C.L., Helman, W.P., and Ross, A.B. (1988). Critical Review of rate constants for reactions of hydrated electrons, hydrogen atoms and hydroxyl radicals ($\cdot OH/\cdot O^-$ in Aqueous Solution. Journal of Physical and Chemical Reference Data *17*, 513–886.

Cao, Y., Qiu, W., Li, J., Zhao, Y., Jiang, J., and Pang, S. (2021). Sulfite enhanced transformation of iopamidol by UV photolysis in the presence of oxygen: Role of oxysulfur radicals. Water Research *189*, 116625.

Chan, T.W., Graham, N.J.D., and Chu, W. (2010). Degradation of iopromide by combined UV irradiation and peroxydisulfate. Journal of Hazardous Materials *181*, 508–513.

Chen, L., Peng, X., Liu, J., Li, J., and Wu, F. (2012). Decolorization of Orange II in

543 Aqueous Solution by an Fe(II)/sulfite System: Replacement of Persulfate. Ind. Eng.
544 Chem. Res. *51*, 13632–13638.
545 Dong, H., Wei, G., Yin, D., and Guan, X. (2020). Mechanistic insight into the generation
546 of reactive oxygen species in sulfite activation with Fe(III) for contaminants
547 degradation. Journal of Hazardous Materials *384*, 121497.
548 Duirk, S.E., Lindell, C., Cornelison, C.C., Kormos, J., Ternes, T.A., Attene-Ramos, M.,
549 Osiol, J., Wagner, E.D., Plewa, M.J., and Richardson, S.D. (2011). Formation of Toxic
550 Iodinated Disinfection By-Products from Compounds Used in Medical Imaging.
551 Environ. Sci. Technol. *45*, 6845–6854.
552 Ens, W., Senner, F., Gygax, B., and Schlotterbeck, G. (2014). Development, validation,
553 and application of a novel LC-MS/MS trace analysis method for the simultaneous
554 quantification of seven iodinated X-ray contrast media and three artificial sweeteners
555 in surface, ground, and drinking water. Anal Bioanal Chem *406*, 2789–2798.
556 Fronaeus, S., Berglund, J., and Elding, L.I. (1998). Iron−Manganese Redox Processes
557 and Synergism in the Mechanism for Manganese-Catalyzed Autoxidation of Hydrogen
558 Sulfite. Inorg. Chem. *37*, 4939–4944.
559 Gara, P.M.D., Bosio, G.N., Gonzalez, M.C., and Mártire, D.O. (2008). Kinetics of the
560 sulfate radical-mediated photo-oxidation of humic substances. International Journal of
561 Chemical Kinetics *40*, 19–24.
562 Guo, Y., Lou, X., Fang, C., Xiao, D., Wang, Z., and Liu, J. (2013). Novel Photo-Sulfite
563 System: Toward Simultaneous Transformations of Inorganic and Organic Pollutants.
564 Environ. Sci. Technol. *47*, 11174–11181.

565 Huie, R.E., and Neta, P. (1984). Chemical behavior of sulfur trioxide(1-) (SO3-) and
566 sulfur pentoxide(1-) (SO5-) radicals in aqueous solutions. J. Phys. Chem. *88*, 5665–
567 5669.
568 Jacobsen, F., Holcman, J., and Sehested, K. (1998). Reactions of the ferryl ion with
569 some compounds found in cloud water. International Journal of Chemical Kinetics *30*,
570 215–221.
571 Jeong, J., Jung, J., Cooper, W.J., and Song, W. (2010). Degradation mechanisms and
572 kinetic studies for the treatment of X-ray contrast media compounds by advanced
573 oxidation/reduction processes. Water Research *44*, 4391–4398.
574 Johnson, R.L., Tratnyek, P.G., and Johnson, R.O. (2008). Persulfate Persistence under
575 Thermal Activation Conditions. Environ. Sci. Technol. *42*, 9350–9356.
576 Kormos, J.L., Schulz, M., and Ternes, T.A. (2011). Occurrence of Iodinated X-ray
577 Contrast Media and Their Biotransformation Products in the Urban Water Cycle.
578 Environ. Sci. Technol. *45*, 8723–8732.
579 Lee, J., von Gunten, U., and Kim, J.-H. (2020). Persulfate-Based Advanced Oxidation:
580 Critical Assessment of Opportunities and Roadblocks. Environ. Sci. Technol. *54*, 3064–
581 3081.
582 Liang, S., Zhu, L., Hua, J., Duan, W., Yang, P.-T., Wang, S.-L., Wei, C., Liu, C., and
583 Feng, C. (2020). Fe2+/HClO Reaction Produces FeIVO2+: An Enhanced Advanced
584 Oxidation Process. Environ. Sci. Technol. *54*, 6406–6414.
585 Lutze, H.V., Bircher, S., Rapp, I., Kerlin, N., Bakkour, R., Geisler, M., von Sonntag, C.,
586 and Schmidt, T.C. (2015). Degradation of Chlorotriazine Pesticides by Sulfate Radicals

587 and the Influence of Organic Matter. Environ. Sci. Technol. *49*, 1673–1680.
588 Mao, Y., Dong, H., Liu, S., Zhang, L., and Qiang, Z. (2020). Accelerated oxidation of
589 iopamidol by ozone/peroxymonosulfate (O3/PMS) process: Kinetics, mechanism, and
590 simultaneous reduction of iodinated disinfection by-product formation potential. Water
591 Research *173*, 115615.
592 Mártire, D.O., Caregnato, P., Furlong, J., Allegretti, P., and Gonzalez, M.C. (2002).
593 Kinetic study of the reactions of oxoiron(IV) with aromatic substrates in aqueous
594 solutions. International Journal of Chemical Kinetics *34*, 488–494.
595 Mottley, C., and Mason, R.P. (1988). Sulfate anion free radical formation by the
596 peroxidation of (Bi)sulfite and its reaction with hydroxyl radical scavengers. Arch
597 Biochem Biophys *267*, 681–689.
598 Neta, P., and Huie, R.E. (1985a). Free-radical chemistry of sulfite. Environ Health
599 Perspect *64*, 209–217.
600 Neta, P., and Huie, R.E. (1985b). One-electron redox reactions involving sulfite ions
601 and aromatic amines. J. Phys. Chem. *89*, 1783–1787.
602 Neta, P., Huie, R.E., and Ross, A.B. (1988). Rate Constants for Reactions of Inorganic
603 Radicals in Aqueous Solution. Journal of Physical and Chemical Reference Data *17*,
604 1027–1284.
605 Pantelaki, I., and Voutsa, D. (2018). Formation of iodinated THMs during chlorination
606 of water and wastewater in the presence of different iodine sources. Science of The
607 Total Environment *613–614*, 389–397.
608 Pérez, S., Eichhorn, P., Celiz, M.D., and Aga, D.S. (2006). Structural Characterization

609 of Metabolites of the X-ray Contrast Agent Iopromide in Activated Sludge Using Ion
610 Trap Mass Spectrometry. Anal. Chem. *78*, 1866–1874.
611 Pestovsky, O., and Bakac, A. (2004). Reactivity of Aqueous Fe(IV) in Hydride and
612 Hydrogen Atom Transfer Reactions. J. Am. Chem. Soc. *126*, 13757–13764.
613 Putschew, A., Wischnack, S., and Jekel, M. (2000). Occurrence of triiodinated X-ray
614 contrast agents in the aquatic environment. Science of The Total Environment *255*,
615 129–134.
616 Richardson, M.J., and Johnston, J.H. (2007). Sorption and binding of nanocrystalline
617 gold by Merino wool fibres—An XPS study. Journal of Colloid and Interface Science
618 *310*, 425–430.
619 Saptari, V. (2003). Fourier transform spectroscopy instrumentation engineering (SPIE
620 Optical Engineering Press Bellingham Washington, DC).
621 Ternes, T.A., and Hirsch, R. (2000). Occurrence and Behavior of X-ray Contrast Media
622 in Sewage Facilities and the Aquatic Environment. Environ. Sci. Technol. *34*, 2741–
623 2748.
624 Ternes, T.A., Stüber, J., Herrmann, N., McDowell, D., Ried, A., Kampmann, M., and
625 Teiser, B. (2003). Ozonation: a tool for removal of pharmaceuticals, contrast media and
626 musk fragrances from wastewater? Water Research *37*, 1976–1982.
627 Tian, F.-X., Xu, B., Lin, Y.-L., Hu, C.-Y., Zhang, T.-Y., Xia, S.-J., Chu, W.-H., and Gao,
628 N.-Y. (2017). Chlor(am)ination of iopamidol: Kinetics, pathways and disinfection by-
629 products formation. Chemosphere *184*, 489–497.
630 Wang, Z., Jiang, J., Pang, S., Zhou, Y., Guan, C., Gao, Y., Li, J., Yang, Y., Qiu, W., and

631 Jiang, C. (2018). Is Sulfate Radical Really Generated from Peroxydisulfate Activated
632 by Iron(II) for Environmental Decontamination? Environ. Sci. Technol. *52*, 11276–
633 11284.
634 Wendel, F.M., Lütke Eversloh, C., Machek, E.J., Duirk, S.E., Plewa, M.J., Richardson,
635 S.D., and Ternes, T.A. (2014). Transformation of Iopamidol during Chlorination.
636 Environ. Sci. Technol. *48*, 12689–12697.
637 Xu, Z., Li, X., Hu, X., and Yin, D. (2017). Distribution and relevance of iodinated X-
638 ray contrast media and iodinated trihalomethanes in an aquatic environment.
639 Chemosphere *184*, 253–260.
640 Yang, T., Wu, S., Liu, C., Liu, Y., Zhang, H., Cheng, H., Wang, L., Guo, L., Li, Y., Liu,
641 M., et al. (2021). Efficient Degradation of Organoarsenic by UV/Chlorine Treatment:
642 Kinetics, Mechanism, Enhanced Arsenic Removal, and Cytotoxicity. Environ. Sci.
643 Technol. *55*, 2037–2047.
644 Yermakov, A.N., and Purmal, A.P. (2003). Iron-Catalyzed Oxidation of Sulfite: From
645 Established Results to a New Understanding. Progress in Reaction Kinetics and
646 Mechanism *28*, 189–256.
647 Yu, Y., Li, S., Peng, X., Yang, S., Zhu, Y., Chen, L., Wu, F., and Mailhot, G. (2016).
648 Efficient oxidation of bisphenol A with oxysulfur radicals generated by iron-catalyzed
649 autoxidation of sulfite at circumneutral pH under UV irradiation. Environ Chem Lett
650 *14*, 527–532.
651 Yuan, Y., Yang, S., Zhou, D., and Wu, F. (2016). A simple Cr(VI)–S(IV)–O2 system for
652 rapid and simultaneous reduction of Cr(VI) and oxidative degradation of organic

653 pollutants. Journal of Hazardous Materials *307*, 294–301.

654 Yuan, Y., Luo, T., Xu, J., Li, J., Wu, F., Brigante, M., and Mailhot, G. (2019). Enhanced
655 oxidation of aniline using Fe(III)-S(IV) system: Role of different oxysulfur radicals.
656 Chemical Engineering Journal *362*, 183–189.

657 Zhao, X., Jiang, J., Pang, S., Guan, C., Li, J., Wang, Z., Ma, J., and Luo, C. (2019).
658 Degradation of iopamidol by three UV-based oxidation processes: Kinetics, pathways,
659 and formation of iodinated disinfection byproducts. Chemosphere *221*, 270–277.

660 Zhou, D., Chen, L., Li, J., and Wu, F. (2018a). Transition metal catalyzed sulfite auto-
661 oxidation systems for oxidative decontamination in waters: A state-of-the-art
662 minireview. Chemical Engineering Journal *346*, 726–738.

663 Zhou, Y., Gao, Y., Pang, S.-Y., Jiang, J., Yang, Y., Ma, J., Yang, Y., Duan, J., and Guo,
664 Q. (2018b). Oxidation of fluoroquinolone antibiotics by peroxymonosulfate without
665 activation: Kinetics, products, and antibacterial deactivation. Water Research *145*, 210–
666 219.

667 Zhou, Y., Jiang, J., Gao, Y., Pang, S.-Y., Ma, J., Duan, J., Guo, Q., Li, J., and Yang, Y.
668 (2018c). Oxidation of steroid estrogens by peroxymonosulfate (PMS) and effect of
669 bromide and chloride ions: Kinetics, products, and modeling. Water Research *138*, 56–
670 66.

671